Cesium adsorption on graphite (0001) surface: The phase diagram

Z. P. Hu,* N. J. Wu,† and A. Ignatiev
Departments of Physics and Chemistry, University of Houston, Houston, Texas 77004
(Received 21 November 1985)

Low-energy electron diffraction (LEED) has been used to study the two-dimensional structure of cesium on the graphite (0001) surface. Six different superstructures have been observed under cesium adsorption: $(\sqrt{7}\times\sqrt{7})$-$R19°$, $2\times2^*$, 2×2, $(\sqrt{3}\times\sqrt{3})$-$R30°$, incommensurate hexagonal and disordered. All but the latter have hexagonal symmetry. The distance between the near-neighbor cesium adatoms in the hexagonally ordered structures decreases from ~ 19 Å for the lowest-exposure incommensurate hexagonal structure measured, to 4.26 Å for the $\sqrt{3}\times\sqrt{3}$-$R30°$ structure. The $\sqrt{3}\times\sqrt{3}$-$R30°$ structure is the most stable structure existing over a coverage range of 0.1 to 0.2 monolayers and a temperature range of 80 to 350 K. A bcc metallic Cs phase has also been observed at high Cs coverages. A limited phase diagram has been generated for cesium adsorption on the (0001) surface of graphite from the LEED data.

INTRODUCTION

Two-dimensional phase transitions have been an attractive research subject for many years. A number of excellent studies have been undertaken in this area,[1–6] with most emphasis placed on physisorption studies of inert-gas atoms on relatively inert substrates, e.g., graphite. Even though physisorption on graphite has been studied quite thoroughly, there is little work on chemisorption on graphite, although much work has been undertaken on the study of two-dimensional behavior in intercalant layers in graphite intercalation compounds.[3–5] The present work is a continuation of past research efforts on alkali-metal chemisorption on low-step-density graphite surfaces and its relation to alkali-metal graphite-intercalation compounds.[7–8] Low-energy electron diffraction (LEED), Auger-electron spectroscopy (AES), and work-function measurements have been used in the present studies to analyze the various surface structures of cesium adsorbed on graphite. Six clearly separated phases for different cesium exposures were observed. These are described below and are used to generate a limited phase diagram for cesium on graphite.

EXPERIMENT

The experiment was undertaken in an ultrahigh-vacuum (UHV) chamber containing a four-grid LEED-AES apparatus, and a universal manipulator with cooling and heating capabilities.[9] A cesium source[10] was installed in the chamber about 11 cm away from the sample with the amount of cesium exposure controlled by adjustment of the electrical current to the source and selection of the exposure time.

A natural graphite crystal was cleaved in air by a high-pressure nitrogen-gas stream and was mounted on the sample holder by a tantalum O-ring. A Chromel-Alumel thermocouple was spot welded onto the O-ring to monitor the temperature of the crystal. For the adsorption studies, a low-step-density area on the graphite (0001) crystal surface was chosen by LEED observation of a threefold-symmetric diffraction pattern.[11]

RESULTS AND DISCUSSION

Upon exposing the graphite sample at 80 K to low coverages of cesium, $0.005<\Theta<0.025$ (here we define Θ as the ratio of the number of Cs atoms on the surface to the number of carbon atoms in a surface layer), small, sharp diffraction rings were observed around the first-order diffraction spots of the graphite (Fig. 1). The radii of the rings increased as the Cs exposure was increased. The ring structure implies that the Cs atoms on the surface

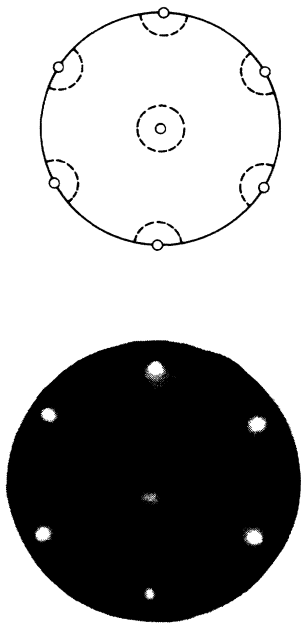

FIG. 1. LEED pattern and schematic for the low-coverage ring structure corresponding to sample 4 in Table I.

have a well-defined nearest-neighbor separation, defined by the ring diameter. The sharpness in k space of the ring (same width as a diffraction spot) implies that the Cs atoms exist in domains on the graphite surface of size much larger than the electron-beam coherence length (>100 Å). Within these domains, the Cs atoms are spaced equidistant from each other probably in a hexagonal array with no orientational ordering with respect to the graphite. The atomic separation in these crystallites decreases uniformly as a function of increased Cs coverage (the diffraction rings expand with increasing coverage) and thus implies that not only are the domains distributed homogeneously and close packed over the graphite surface, but that repulsive forces are dominant between the Cs adatoms at these low coverages. Within this incommensurate hexagonal structure model, Cs coverage can be determined and is given for this disordered structure in Table I.

At a coverage near $\Theta=0.07$, a $(\sqrt{7}\times\sqrt{7})$-$R19.11°$ pattern was observed (Fig. 2). The angle between the lattice vectors of the overlayer and that of the substrate is $\sim 19°$ for this structure. Two oppositely rotated domains of Cs atoms cause the two sets of sixfold symmetric diffraction spots with $\sim 38°$ relative orientation angle between the domains, as seen in Fig. 3. The nearest-neighbor distance of the Cs atoms in this structure, assuming a single Cs atom per surface lattice basis, is 6.5 Å. This large spacing supports the concept that repulsive forces dominate the Cs interaction on the graphite surface at low coverage. The $(\sqrt{7}\times\sqrt{7})$-$R19.11°$ phase existed in a temperature range from 80 to 180 K. Above 180 K, the diffraction pattern disappeared, e.g., the surface disordered with the phase transition being irreversible.

In the case of Cs exposure at 80 K and coverage $0.08<\Theta<0.11$, an incommensurate Cs/graphite structure with orientational ordering[12,13] appeared. As the lattice parameter and structure are very similar to a 2×2 structure, we have denoted this phase as $2\times2^*$ (Fig. 4), and have described the orientational ordering exhibited by the structure.[14] The $2\times2^*$ phase exists over the temperature range of liquid nitrogen (LNT) to ~ 80 K. Above 150 K, the phase transforms to a $(\sqrt{3}\times\sqrt{3})$-$R30°$ structure in an irreversible manner.

When more Cs atoms are evaporated onto the $2\times2^*$ structure at 80 K, the $2\times2^*$ phase converts to a 2×2 phase (Fig. 5). The 2×2 structure is one of relatively high Cs density ($\Theta\approx0.1$). This forces the adatoms to overcome the repulsive interaction seen for the ring structures and the $(\sqrt{7}\times\sqrt{7})$-$R19°$ and $2\times2^*$ structures, and to populate high-symmetry positions on the graphite surface that are closer than the nearest-neighbor Cs distance in metallic Cs. In the 2×2 phase, the distance between adatoms as obtained from the LEED pattern, again assuming a single Cs atom basis per lattice point, is 4.92 Å (compared to 5.24 Å for metallic Cs) and the phase only exists in temperature range of from 80 to 120 K. Above 120 K, the 2×2 phase converts to the $(\sqrt{3}\times\sqrt{3})$-$R30°$ phase.

The $(\sqrt{3}\times\sqrt{3})$-$R30°$ phase can be obtained by either direct evaporation of a large amount of Cs onto the graphite at 80 K, or by phase transition from the 2×2 or

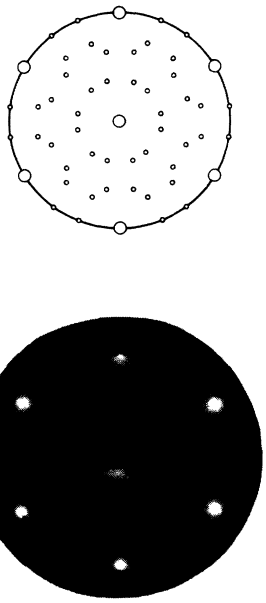

FIG. 2. LEED pattern and schematic for the $(\sqrt{7}\times\sqrt{7})$-$R19°$ structure; two domains are present.

TABLE I. Coverage data for observed cesium ring structures. γ is the ratio of diffraction ring diameter to the distance between two directly opposite graphite diffraction spots, d is the mean distance between two Cs adatoms on the graphite surface, N is the Cs density on the surface, and Θ is the coverage of Cs on the surface.

Structure number	γ	d (Å)	N (10^{-14} atom/cm^2)	Θ
1	0.13	18.9	0.32	0.008
2	0.15	16.4	0.43	0.011
3	0.16	15.4	0.49	0.013
4	0.18	13.7	0.61	0.016
5	0.20	12.3	0.76	0.02

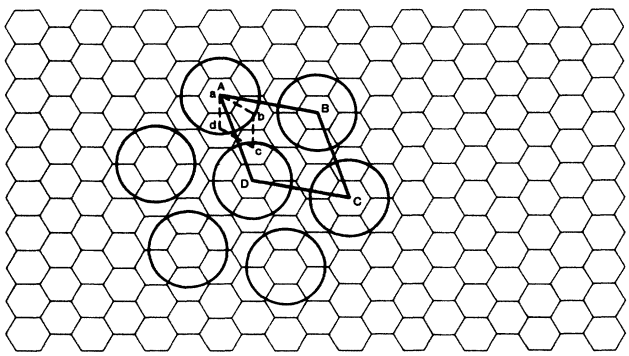

FIG. 3. Proposed real-space structure for the $(\sqrt{7}\times\sqrt{7})$-$R19°$ Cs/graphite assuming one Cs atom per surface lattice point located in the graphite honeycomb hollow. $abcd$ is the graphite-surface unit cell; $ABCD$ is the $(\sqrt{7}\times\sqrt{7})$-$R19°$ unit cell. A second domain is obtained by rotating by 38°.

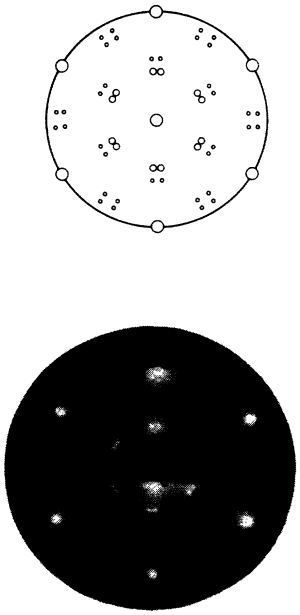

FIG. 4. LEED pattern and schematic for the $2\times2^*$ structure.

$2\times2^*$ structures. An increase of temperature to approximately 150 K, or exposure to an electron beam (at a dose of approximately 1×10^{18} electrons/cm^2) converts the 2×2 and the $2\times2^*$ phases irreversibly to the $(\sqrt{3}\times\sqrt{3})$-$R30°$ phase. The $(\sqrt{3}\times\sqrt{3})$-$R30°$ phase is the most stable phase for cesium on graphite and can be observed at coverages from $\Theta=0.1$ to 0.22 and over a temperature range of 80 to 350 K. In the simple one atom per lattice point surface structure model, the nearest-neighbor distance (assumed to be the Cs atom diameter) in the $(\sqrt{3}\times\sqrt{3})$-$R30°$ structure is 4.26 Å, which is much smaller than that in metallic Cs (5.24 Å) but larger than the ionic diameter of cesium (3.38 Å).

A similar large decrease in atomic diameter (over that of the metallic phase) has been observed for potassium on graphite,[15] and is probably due to a large amount of charge transfer from the alkali to the graphite.

The $(\sqrt{3}\times\sqrt{3})$-$R30°$ can also be obtained by direct evaporation of Cs to exposures of $\sim1\times10^{14}$ Cs atoms/cm^2 with the substrate graphite at 80 K. Under these conditions, the $(\sqrt{3}\times\sqrt{3})$-$R30°$ pattern is accompanied by a diffuse diffraction ring going through the $\sqrt{3}$ diffraction beams (Fig. 6) which disappears upon exposure to the electron beam. This beam-induced increase in surface order may be due to either ordering of the ring to the $(\sqrt{3}\times\sqrt{3})$-$R30°$ structure, or electron-stimulated desorption (ESD) of rotationally disordered Cs, responsible for the ring structure. ESD was observed for potassium in the 2×2 phase on graphite.[16]

For the $(\sqrt{3}\times\sqrt{3})$-$R30°$ structure at a coverage of $\Theta=0.1$–0.15, additional exposure to Cs at 80 K results in the formation of the $2\times2^*$ (or at times the 2×2) structure. This is the only region of coexistence observed and is removed by heating to ~150 K or exposure to an electron beam (again at an exposure of $\sim1\times10^{18}$ electrons/cm^2). All the phase transitions observed in this $(\sqrt{3}\times\sqrt{3})$-$R30°$ system are irreversible, i.e., once the $(\sqrt{3}\times\sqrt{3})$-$R30°$ phase is formed, the system will not convert to another phase.

When more than one monolayer equivalent of Cs atoms was evaporated onto the graphite surface, the $(\sqrt{3}\times\sqrt{3})$-$R30°$ pattern became diffuse and disappeared. When this

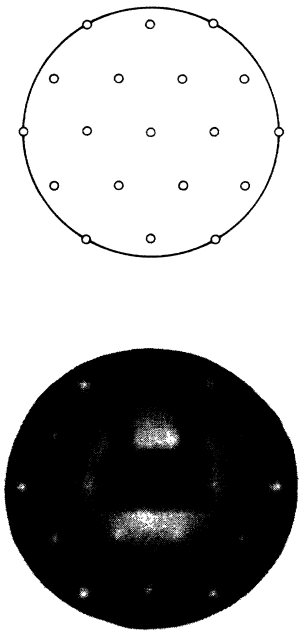

FIG. 5. LEED pattern and schematic for the 2×2 structure.

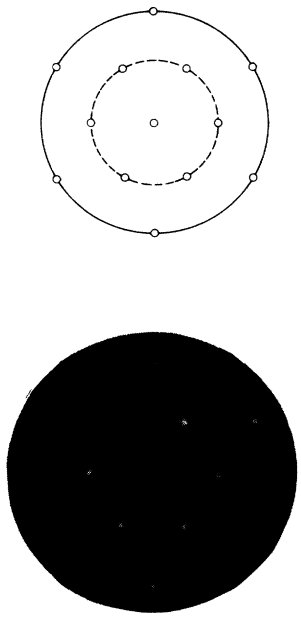

FIG. 6. LEED pattern and schematic for the $(\sqrt{3}\times\sqrt{30})$-$R19°$ structure. Note the diffuse scattering ring in the pattern.

high-coverage diffuse scattering system was left at room temperature for longer than ~ 8 h and then cooled to 80 K, an ordered structure appeared on the graphite surface (Fig. 7). This structure was oriented with respect to the substrate graphite, and was analyzed (again, under the assumption of one Cs atom per overlayer lattice point) to be due to an incommensurate bcc overlayer of Cs on the graphite (Fig. 8). The bcc lattice parameter extracted from the diffraction pattern is 5.8 ± 0.2 Å, which is in good agreement with $a_0 = 6.045$ Å for bcc Cs. The two domains of the cubic Cs stem from the two observed 30° rotated domains of the substrate graphite (a total of 12 weak diffraction spots at the outer edge of diffraction pattern in Fig. 7). The reason for the existence of the graphite domains is not fully understood; however, the domain formation may be the result of Cs intercalation into the first graphite layer.

This metallic structure is very sensitive to exposure to the electron beam. An exposure of $\sim 1 \times 10^{14}$ electrons/cm^2 at 50 eV disordered the structure and hence prevented detailed LEED analysis. The cubic metallic phase, can, however exist indefinitely at 120 K without exposure to the electron beam. A metallic phase was also observed for lithium adsorption on (0001) graphite,[7] although it occurred in the hexagonal and not the cubic structure. In addition, there was no orientational ordering observed for the Li metallic phase. It is well to note again that the Cs cubic metallic phase is only observed under exposures of greater than ~ 1- to 2-monolayer equivalents of Cs and then only after long-term room-temperature annealling and subsequent cooling to 80 K.

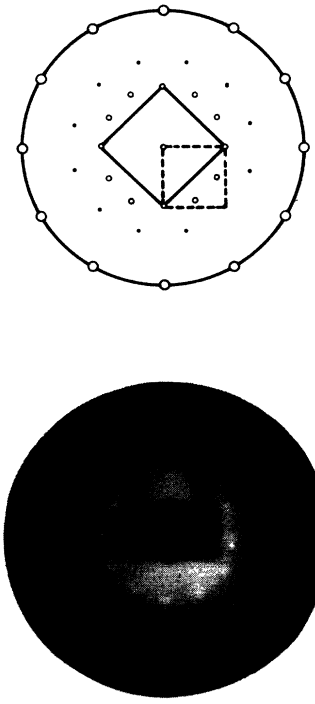

FIG. 7. LEED pattern and schematic for the Cs metallic structure. The primitive and centered cells are shown for only one domain. The remaining diffracted beams are due to two additional domains rotated at ±60° from the one shown.

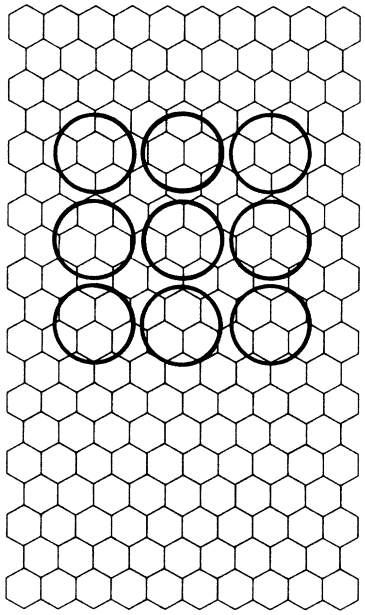

FIG. 8. Proposed real-space structure for the orientation of the bcc metallic Cs overlayer on graphite. Two additional domains observed in the pattern of Fig. 7 would be obtained by rotation of this structure by ±60°. Note that the Cs overlayer is not commensurate.

LEED I-V—curve dynamical analysis is currently underway with respect to the (2×2) and $(\sqrt{3}\times\sqrt{3})$-$R30°$ structures; however, from preliminary results following the LEED arguments given in the analysis of Li on graphite,[7] it can be stated here that the Cs phases reported above (except the metallic phase) are not due to Cs intercalation into graphite. The structures are, therefore, a result of Cs two-dimensional (2D) layers *on* graphite for

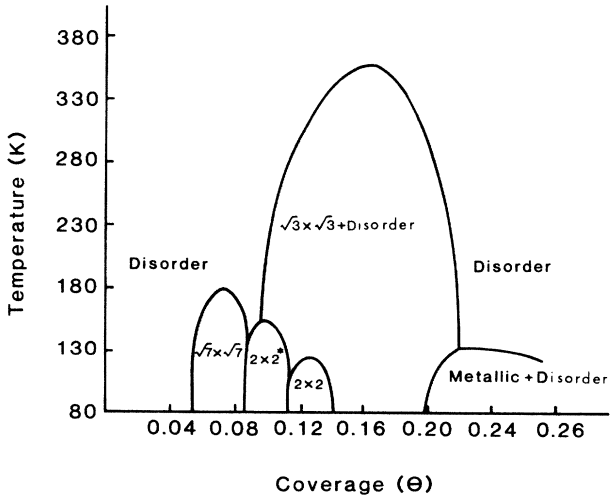

FIG. 9. Phase diagram in temperature and coverage space for cesium adsorbed on the graphite (0001) surface.

which a limited phase diagram has been generated (Fig. 9). Within the phase diagram, $(\sqrt{7}\times\sqrt{7})$-$R19°$ and 2×2 phases have been observed for Cs intercalated graphite,[3,4] however, the nonhexagonal $\sqrt{3}\times2$ and $\sqrt{3}\times\sqrt{13}$ phases reported for the intercalated case [5] have not been observed in the present study of Cs on the (0001) surface of graphite.

One other point to make is that in the low-coverage limit ($\Theta<0.14$) at 80 K, the structures observed [incommensurate hexagonal, $(\sqrt{7}\times\sqrt{7})$-$R19°$, 2×2, and the orientational ordering $2\times2^*$ structures] indicate dominant repulsive interactions between near-neighbor Cs adatoms with a characteristic nearest-neighbor distance of greater than ~4.9 Å. The addition of a small amount of energy to the system through heating, however, results (for exposures $0.1<\Theta<0.14$) in transition to the $(\sqrt{3}\times\sqrt{3})$-$R30°$ structure with a nearest-neighbor distance of 4.27 Å and dominant attractive near-neighbor interactions.

SUMMARY

The adsorption of cesium onto the (0001) surface of graphite results in six different 2D superstructures: incommensurate hexagonal, $(\sqrt{7}\times\sqrt{7})$-$R19°$, $2\times2^*$, 2×2, $(\sqrt{3}\times\sqrt{3})$-$R30°$, and disordered. The phase transitions from these structures have been observed and have been noted to be irreversible. The $(\sqrt{3}\times\sqrt{3})$-$R30°$ structure is the most stable existing in a coverage range of $0.1<\Theta<0.22$ and a temperature range of 80 to 350 K. A limited phase diagram for the 2D cesium system has been generated. A bcc metallic Cs overlayer has also been observed to form under coverages of 1—2 monolayers equivalent of Cs.

ACKNOWLEDGMENTS

Helpful discussions with S. C. Moss are gratefully acknowledged. Partial support for this work was supplied by the R. A. Welch Foundation.

---

*Permanent address: University of Science and Technology, Hafei, China.

†Permanent address: Institute of Physics, Academy of Sciences, Beijing, China.

[1]S. C. Fain, Jr., M. D. Chinn, and R. D. Diehl, Phys. Rev. B **21**, 4170 (1980).

[2]J. J. Lander and J. Morrison, Surf. Sci. **6**, 1 (1967).

[3]A. N. Berker, N. Kambe, G. Dresselhaus, and M. S. Dresselhaus, Phys. Rev. Lett. **45**, 1452 (1980).

[4]R. Clarke, N. Caswell, S. A. Solin, and P. M. Horn, Phys. Rev. Lett. **43**, 2018 (1979).

[5]D. W. Hwang, N. W. Parker, M. Utlaut, and A. V. Crewe, Phys. Rev. B **27**, 1458 (1983).

[6]M. F. Toney and S. C. Fain, Jr., J. Vac. Sci. Technol. A **2**, 898 (1984).

[7]Z. P. Hu and A. Ignatiev, Phsy. Rev. B **30**, 4856 (1984).

[8]N. J. Wu and A. Ignatiev, Phys. Rev. B **28**, 7288 (1983).

[9]N. J. Wu and A. Ignatiev, Rev. Sci. Instrum. **56**, 752 (1985).

[10]Saes Getters, Inc., model NF/8/825/T14-14.

[11]N. J. Wu and A. Ignatiev, Phys. Rev. B **25**, 2983 (1982).

[12]A. D. Novaco and J. P. McTague, Phys. Rev. Lett. **38**, 1286 (1977).

[13]C. R. Fuselier, J. C. Raich, and N. S. Gillis, Surf. Sci. **92**, 667 (1980).

[14]Z. P. Hu, N. J. Wu, and A. Ignatiev (unpublished).

[15]A. Ignatiev and W. C. Fan, J. Vac. Sci. Technol. (to be published).

[16]N. J. Wu and A. Ignatiev, J. Vac. Sci. Technol. **20**, 896 (1982).

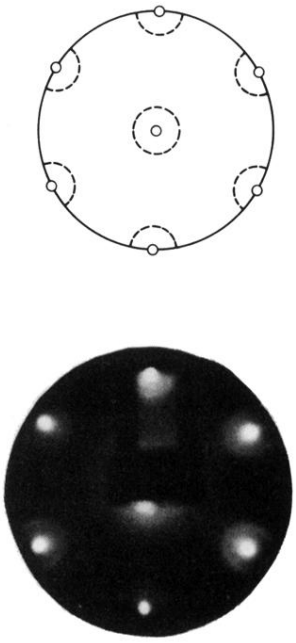

FIG. 1. LEED pattern and schematic for the low-coverage ring structure corresponding to sample 4 in Table I.

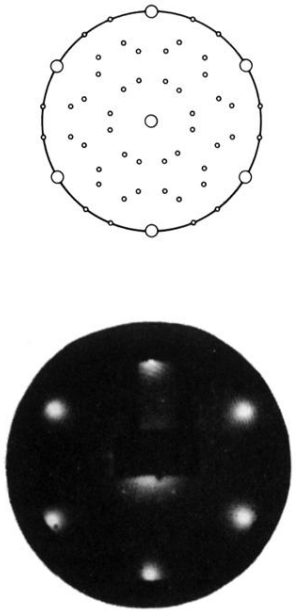

FIG. 2. LEED pattern and schematic for the $(\sqrt{7}\times\sqrt{7})$-$R19°$ structure; two domains are present.

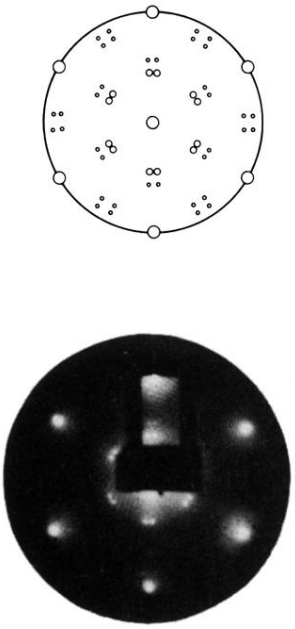

FIG. 4. LEED pattern and schematic for the $2\times2^{*}$ structure.

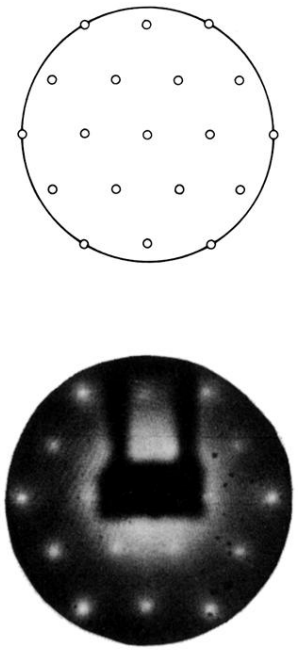

FIG. 5. LEED pattern and schematic for the 2×2 structure.

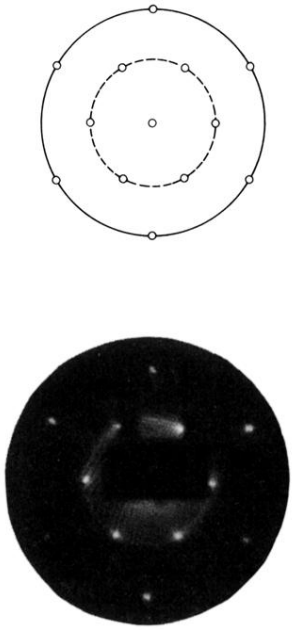

FIG. 6. LEED pattern and schematic for the $(\sqrt{3}\times\sqrt{30})$-$R19°$ structure. Note the diffuse scattering ring in the pattern.

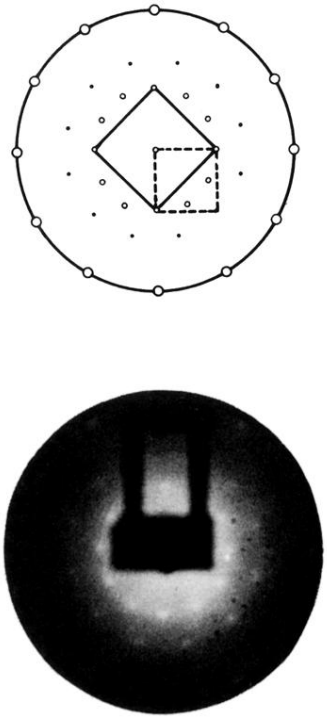

FIG. 7. LEED pattern and schematic for the Cs metallic structure. The primitive and centered cells are shown for only one domain. The remaining diffracted beams are due to two additional domains rotated at $\pm 60°$ from the one shown.